Stable light-bullet solutions in the harmonic and parity-time-symmetric potentials

Chao-Qing Dai (戴朝卿),[1,2] Xiao-Gang Wang (汪小刚),[1] and Guo-Quan Zhou (周国泉)[1]
[1]*School of Sciences, Zhejiang Agriculture and Forestry University, Lin'an, Zhejiang 311300, People's Republic of China*
[2]*Optical Sciences Group, Research School of Physics and Engineering, The Australian National University, Canberra ACT 0200, Australia*
(Received 17 November 2013; published 24 January 2014)

Analytical light-bullet solutions of a $(3+1)$-dimensional nonlinear Schrödinger equation with inhomogeneous diffraction or dispersion and nonlinearity in the presence of the harmonic and parity-time-symmetric potentials are explored. Diffraction or dispersion and nonlinearity play important roles in the evolutional characteristics such as amplitude, width, and phase. The compression and broadening behaviors of light bullets are discussed and compared in the exponential, Gaussian and hyperbolic diffraction or dispersion decreasing media and the periodic distributed amplification system. Moreover, phase changes of light bullets in different systems are also illustrated.

DOI: 10.1103/PhysRevA.89.013834 PACS number(s): 42.81.Dp, 05.45.Yv, 42.65.Tg

I. INTRODUCTION

In classical quantum mechanics, Hermiticity of every operator is associated with a physical observable. In 1998, the pioneering work of Bender and co-workers [1] reported that fundamental physical symmetries such as parity (P) and time (T) reversal may be sufficient (in suitable parametric regimes) to ensure that the eigenvalues of the Hamiltonian are real. The Hamiltonian H is invariant neither under parity operator $\widehat{P}$, which is defined by the spatial reflection relations $p\rightarrow -p$ and $x\rightarrow -x$ (p and x stand for momentum and position operators, respectively), nor under the time-reversal operator $\widehat{T}$ by $p\rightarrow -p$, $x\rightarrow x$, and $i\rightarrow -i$. Therefore, the PT symmetric potential satisfies $V(\mathbf{r})=V^*(-\mathbf{r})$, with $*$ denoting complex conjugation [1,2]; that is, the real component of a PT complex potential must be a symmetric function of position, whereas the imaginary part should be antisymmetric.

Owing to the mathematical correspondence between the quantum Schrödinger equation and the paraxial equation of diffraction [nonlinear Schrödinger equation (NLSE)], the concept of PT symmetry has been introduced in the field of optics in recent years. The role of potential $V(\mathbf{r})$ in quantum mechanics can be played as an optical potential in optics by a complex refractive-index distribution $n(\mathbf{r})=n_R(\mathbf{r})+\mathrm{i}n_I(\mathbf{r})$, wherein the real component $n_R(\mathbf{r})$ describes the refractive-index profile, while the imaginary part $n_I(\mathbf{r})$ denotes the gain $(+)$ or loss $(-)$ in the system. In optics, the complex refractive-index distribution obeys the condition $n(\mathbf{r})=n^*(-\mathbf{r})$, namely, PT-symmetric conditions imply $n_R(\mathbf{r})=n_R(-\mathbf{r})$ and $n_I(\mathbf{r})=-n_I(-\mathbf{r})$, which indicates that the index distribution must be an even function of position, whereas the gain and loss must be an odd function.

In standard quantum well semiconductor lasers or semiconductor optical amplifiers and photorefractive crystals, gain or loss levels are approximately $\pm 40\ \mathrm{cm}^{-1}$ at wavelengths approximately to 1 μm. These typical values are sufficient to observe PT behavior [3,4]. Moreover, cubic, quadratic, and photorefractive nonlinearity conditions in optics also provide an additional degree of freedom to observe PT behavior [3,5]. In nonlinear optics, Musslimani *et al.* [5] was the first research group to realize optical spatial solitons in PT-symmetric potentials. The proposed PT systems can be realistically implemented through a judicious inclusion of gain or loss regions in optical waveguides [6]. More recently, optical PT symmetry was experimentally observed in two-element coupled systems composed of waveguides with gain and loss [7,8].

Quite recently, soliton propagations in optical media with PT symmetry are presently attracting great interest both from the theoretical and from the applicative points of view. The PT symmetry can lead to altogether new optical dynamics, such as abrupt phase transitions [9], the appearance of power oscillations, and secondary emissions [6], etc. Optical solitons in PT-symmetric periodic potentials were investigated [10]. Stable bright spatial solitons in defocusing Kerr media with PT-symmetric potentials have also been reported [11]. Dark solitons and vortices in PT-symmetric nonlinear media were discussed, too [12]. Two-dimensional (2D) solitons in defocusing Kerr media [11] and nonlocal media [13] with PT-symmetric potentials have been exhibited.

Spatiotemporal localized structures such as optical soliton [14,15], similariton [16,17], rogue wave [18], and light bullet (LB) [19,20] have been a subject of intense investigation in long-distance communication and all-optical ultrafast switching devices. Spatiotemporal solitons or bullets may be understood as the result of the simultaneous balance of diffraction and group velocity dispersion (GVD) by the transverse self-focusing and nonlinear phase modulation in the longitudinal direction, respectively [21]. Many of these spatiotemporal localized structures are nonautonomous (this terminology was presented first by Serkin [22,23]). However, spatiotemporal localized structures in PT-symmetric potentials are relatively less reported.

In this present paper, we first obtain LB solutions based on a $(3+1)$-dimensional (3D) variable-coefficient NLSE in harmonic and PT-symmetric potentials and discuss the dynamical behaviors of LB in different diffraction or dispersion decreasing media (DDM). The stability of these LB solutions is also investigated. These results may provide alternative methods in potential applications of synthetic PT-symmetric systems.

II. MODEL AND TRANSFORMATION

The 3D variable-coefficient NLSE in harmonic and PT-symmetric potentials has the form

$$\mathrm{i}u_z+\frac{\beta(z)}{2}(\triangle_\perp u+u_{tt})+\chi(z)|u|^2u+\gamma(z)r^2u+U_{PT}u=0, \tag{1}$$

where $\triangle_\perp = (\partial_x^2, \partial_y^2)$, $\mathbf{r} \equiv (x,y,t)$, the complex envelope of the electrical field $u(z,\mathbf{r})$, longitudinal z and transverse x,y coordinates, and comoving time t are respectively normalized as $(k_0 w_0)^{-1}(n_2/n_0)^{-1/2}$, the diffraction length $L_D \equiv k_0 w_0^2$, with the input width unit w_0 with the wave number $k_0 \equiv 2\pi n_0/\lambda$ at the input wavelength λ and $\sqrt{L_D}$. All coordinates are made dimensionless by the choice of coefficients. Variable coefficients $\beta(z)$, $\chi(z)$, and $\gamma(z)$ represent the diffraction or dispersion, nonlinearity, and harmonica potential coefficients, respectively. The complex PT-symmetric potential $U_{PT}(z,\mathbf{r}) = v(z,\mathbf{r}) + i\,w(z,\mathbf{r})$. Even function $v(z,\mathbf{r}) \equiv k_0^2 w_0^2 n_R(z,\mathbf{r})$ and odd function $w(z,\mathbf{r}) \equiv k_0^2 w_0^2 n_I(z,\mathbf{r})$ are the real and imaginary components of the complex PT-symmetric potential, respectively, and correspond to the index guiding and the gain or loss distribution of the optical potential, respectively.

In the context of the Bose-Einstein condensate, Eq. (1), exchanging z and t, is also called the Gross-Pitaevskii equation, which governs the evolution of matter waves. If $v = 0, w = \gamma(z)$, the model in [24–26] can be recovered. If $\gamma = 0, v = 0, w = \gamma(z)$, Eq. (1) governs the propagation of LB in [19]. When β and χ are both constant and $\gamma = 0$, Eq. (1) is the governing equation in [20]. When β is a constant and $v = 0, w = \gamma(z)$, Eq. (1) is the corresponding model in [27].

In order to derive the analytical LB solutions for Eq. (1), substituting the transformation

$$u(z,\mathbf{r}) = \rho_0 \omega^{-3/2} U(Z,X,Y,T) \exp[i\omega_z r^2/(2\beta\omega)], \tag{2}$$

with

$$Z = \int_0^z \frac{\beta(s)}{B\omega(s)} dz, \omega(z) = \frac{\rho_0^2 B\chi(z)}{G\beta(z)}, \tag{3}$$

$$X = \frac{x}{\omega(z)}, \quad Y = \frac{y}{\omega(z)}, \quad T = \frac{t}{\omega(z)}, \tag{4}$$

into Eq. (1) yields a simpler NLSE,

$$iU_Z + \frac{B}{2}(U_{XX} + U_{YY} + U_{TT}) + G|U|^2 U + V_{PT} U = 0, \tag{5}$$

with $V_{PT}(X,Y,T) = V(X,Y,T) + i\,W(X,Y,T)$ and two constants B and G.

Further, variable coefficients in Eq. (1) exist the following constraints as follows:

$$\gamma(z) = \frac{\beta\omega_{zz} - \beta_z\omega_z}{2\beta^2\omega}, \tag{6}$$

and

$$v(z,x,y,t) = \frac{\beta(z)}{B\omega(z)} V(X,Y,T),$$
$$w(z,x,y,t) = \frac{\beta(z)}{B\omega(z)} W(X,Y,T). \tag{7}$$

From this relation (2), we know that solutions of Eq. (5) can be as seeds to generate various solutions of Eq. (1) under conditions (6) and (7). Note that functions v and w must satisfy the restraint of even and odd functions, which make the equation more difficult to solve. Therefore, it is very important to obtain soliton solutions of Eq. (5).

III. SOLUTIONS TO THE SIMPLER NLSE

We seek a solution of the 3D NLSE (5) in the form

$$U(Z,X,Y,T) = \Phi(X,Y,T) \exp[i\lambda Z + i\Theta(X,Y,T)], \tag{8}$$

where Φ and Θ are real valued functions that satisfy the following differential equations:

$$\frac{B}{2}(\triangle\Phi - |\nabla\Theta|^2\Phi) + V(X,Y,T)\Phi + G\Phi^3 = \lambda\Phi, \tag{9}$$

$$\frac{B}{2}\Phi\triangle\Theta + B\nabla\Theta\cdot\nabla\Phi + W(X,Y,T)\Phi = 0. \tag{10}$$

First, we consider the complex PT-symmetric potential of the Scarff II type in three dimensional extension as

$$V(X,Y,T) = \left(2 + W_0^2/9\right)[\mathrm{sech}^2(X) + \mathrm{sech}^2(Y) + \mathrm{sech}^2(T)] + \left(V_0^2 - 2 - W_0^2/9\right)\mathrm{sech}^2(X)\mathrm{sech}^2(Y)\mathrm{sech}^2(T) \tag{11}$$

and

$$W(X,Y,T) = W_0[\mathrm{sech}(X)\tanh(X) + \mathrm{sech}(Y)\tanh(Y) + \mathrm{sech}(T)\tanh(T)], \tag{12}$$

which satisfies the properties of PT symmetry: $V(X,Y,T) = V(-X,-Y,-T)$ and $W(X,Y,T) = -W(-X,-Y,-T)$. This PT-symmetric potential is an extension of the corresponding potential in [11,28].

A bound-state nonlinear solution to Eqs. (9) and (10) must satisfy the localization condition $\Phi \to 0$ as $(X,Y,T) \to \pm\infty$. Thus, we can derive

$$\Phi(X,Y,T) = \pm\sqrt{\frac{18 + W_0^2 - 9V_0^2}{9G}}\,\mathrm{sech}(X)\mathrm{sech}(Y)\mathrm{sech}(T) \tag{13}$$

$$\Theta(X,Y,T) = \frac{W_0}{3}\{\arctan[\sinh(X)] + \arctan[\sinh(Y)] + \arctan[\sinh(T)]\}, \tag{14}$$

with constant $B = 2$, $\lambda = 3$ and two arbitrary constants V_0 and W_0.

Therefore, Eq. (5) possesses the following soliton solution

$$U = \pm\sqrt{\frac{18 + W_0^2 - 9V_0^2}{9G}}\,\mathrm{sech}(X)\mathrm{sech}(Y)\mathrm{sech}(T) \times \exp\{i[3Z + \Theta(X,Y,T)]\}, \tag{15}$$

where $\Theta(X,Y,T)$ is given by Eq. (14).

Moreover, Eq. (5) also admits a solution,

$$U = \pm\sqrt{\frac{-V_2}{G}}\,\mathrm{sech}(X)\mathrm{sech}(Y)\mathrm{sech}(T) \times \exp\left(i\left\{\frac{3B}{2}Z \pm \sqrt{\frac{2V_1}{B}}[\tanh(X) + \tanh(Y) + \tanh(T)]\right\}\right), \tag{16}$$

under the complex PT-symmetric potential

$$V = B[\mathrm{sech}^2(X) + \mathrm{sech}^2(Y) + \mathrm{sech}^2(T)] + V_1[\mathrm{sech}^4(X) + \mathrm{sech}^4(Y) + \mathrm{sech}^4(T)] + V_2\mathrm{sech}^2(X)\mathrm{sech}^2(Y)\mathrm{sech}^2(T) \tag{17}$$

and

$$W = \pm 2\sqrt{2BV_1}[\mathrm{sech}^2(X)\tanh(X) + \mathrm{sech}^2(Y)\tanh(Y) + \mathrm{sech}^2(T)\tanh(T)], \tag{18}$$

with two arbitrary constants V_1 and V_2.

Solution (15) exists in self-focusing media ($G > 0$) in Eq. (5) (positive nonlinearity) if $18 + W_0^2 - 9V_0^2 > 0$, as well as in self-defocusing media ($G < 0$) in Eq. (5) (negative nonlinearity) if $18 + W_0^2 - 9V_0^2 < 0$. Similarly, solution (16) exists also in both self-focusing and self-defocusing media. For $B > 0, G > 0$ in self-focusing media, solution (16) is reasonable for $V_1 > 0, V_2 < 0$, while solution (16) exists for $B > 0, G < 0$ in self-defocusing media if $V_1 > 0, V_2 > 0$. This PT-symmetric potential is also a 3D extension of the corresponding potential in [28].

Note that an abrupt phase transition, which is a new optical dynamic in PT symmetry, can also be found in solutions (15) and (16). Figure 1(a) is an isosurface plot of the phase transition for solution (16). Two kinds of abrupt phase transitions corresponding to the positive and negative signs for solution (16) in the X-Y plane are shown in Fig. 1. In this first case in Fig. 1(b), phase transit from the bigger value in positive X or Y axis to the smaller value in negative X or Y axis. The second case in Fig. 1(c) is opposite, that is, phase transit from the bigger value in negative X or Y axis to the smaller value in positive X or Y axis. The phase transition of solution (15) is similar to that in Fig. 1(b). The letter "P" in Figs. 1(b) and 1(c) denotes "phase," and this notation also appears in Figs. 2(e), 4(a), and 4(b).

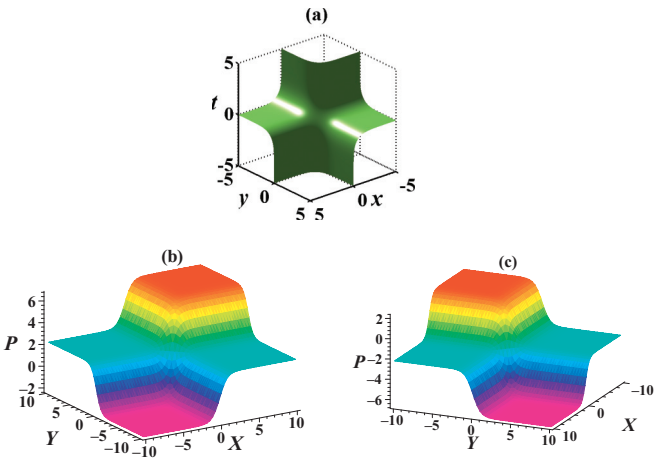

FIG. 1. (Color online) (a) Isosurface plot of phase for Eq. (16). (b),(c) Two kinds of abrupt phase transitions corresponding to the positive and negative signs for Eq. (16), respectively. The other parameters are chosen as $V_1 = 10, B = 2$ at $Z = 0$.

IV. DYNAMICAL BEHAVIORS OF LBS

From the transformation (2) and solutions (15) and (16), we can obtain LBs for Eq. (1) under the PT-symmetrical potentials (7) with Eqs. (11) and (12) and Eqs. (17) and (18). The peak and width of LBs is related to $\rho_0\omega^{-3/2}(z)$ and $\omega(z)$ with $\rho_0^2 B\chi(z)/[G\beta(z)]$, respectively, and the chirp of phase is expressed by $\omega_z/[2\beta(z)\omega(z)]$. These factors show that diffraction or dispersion parameter $\beta(z)$ and nonlinearity parameter $\chi(z)$ strongly influence evolutional characteristics of LBs including amplitude, width, and phase. Here we discuss the compressed and broadened behaviors of LBs to self-focusing and self-defocusing cases in different media.

We next discuss these behaviors in self-focusing media. The first case is a medium with decreasing exponential diffraction or dispersion $\beta(z) = \beta_0 \exp(-\delta z)$, $\chi(z) = \chi_0 \exp(-\delta z - \sigma z)$ [29,30], where β_0 and δ are related to diffraction or dispersion, $\delta > 0$ corresponds to DDM. χ_0 and σ are the parameters to describe the nonlinearity. When $\sigma > 0$, the solution above can be applied to the problem of soliton propagating in optical fiber amplifiers. For $\sigma < 0$, solution above has application to the soliton management communication links where fiber losses are compensated periodically by an amplification system.

As shown in Figs. 2(a) and 2(b), the complex PT-symmetric potential (7) with (11) and (12) in DDM satisfies the properties of even and odd functions, respectively, with regards to x, y and t; that is, $v(x,y,t) = v(-x,-y,-t)$ and $w(x,y,t) = -w(-x,-y,-t)$. Under this potential, the spatiotemporal localized LB (2) with (15) shown in

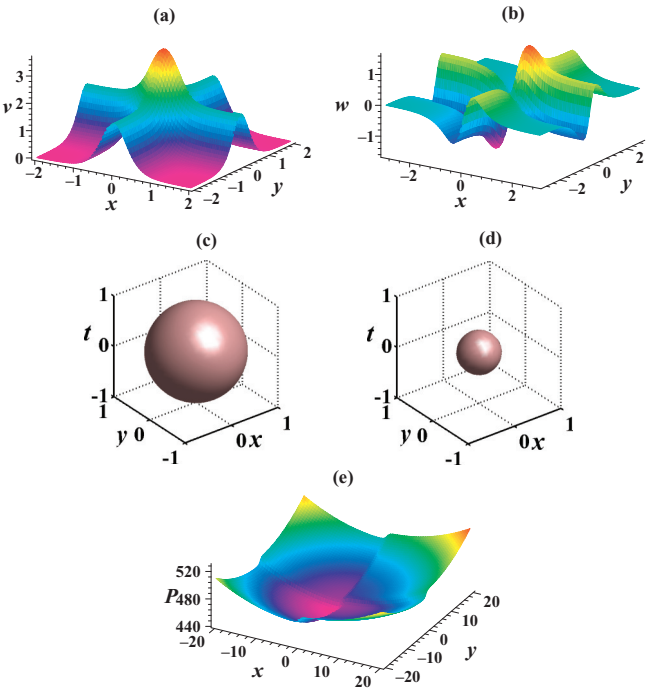

FIG. 2. (Color online) The profiles of (a) even function v and (b) odd function w at $t = 10$ in DDM. Isosurface plots of compressed LBs in DDM at (c) $z = 0$ and (d) $z = 50$. (e) Phase change corresponding to (d). The parameters are chosen as $\beta_0 = 0.5, \chi_0 = 0.3, \delta = 0.025, \sigma = 0.02, B = 2, G = 1, \rho_0 = 1, W_0 = 10, V_0 = 3$.

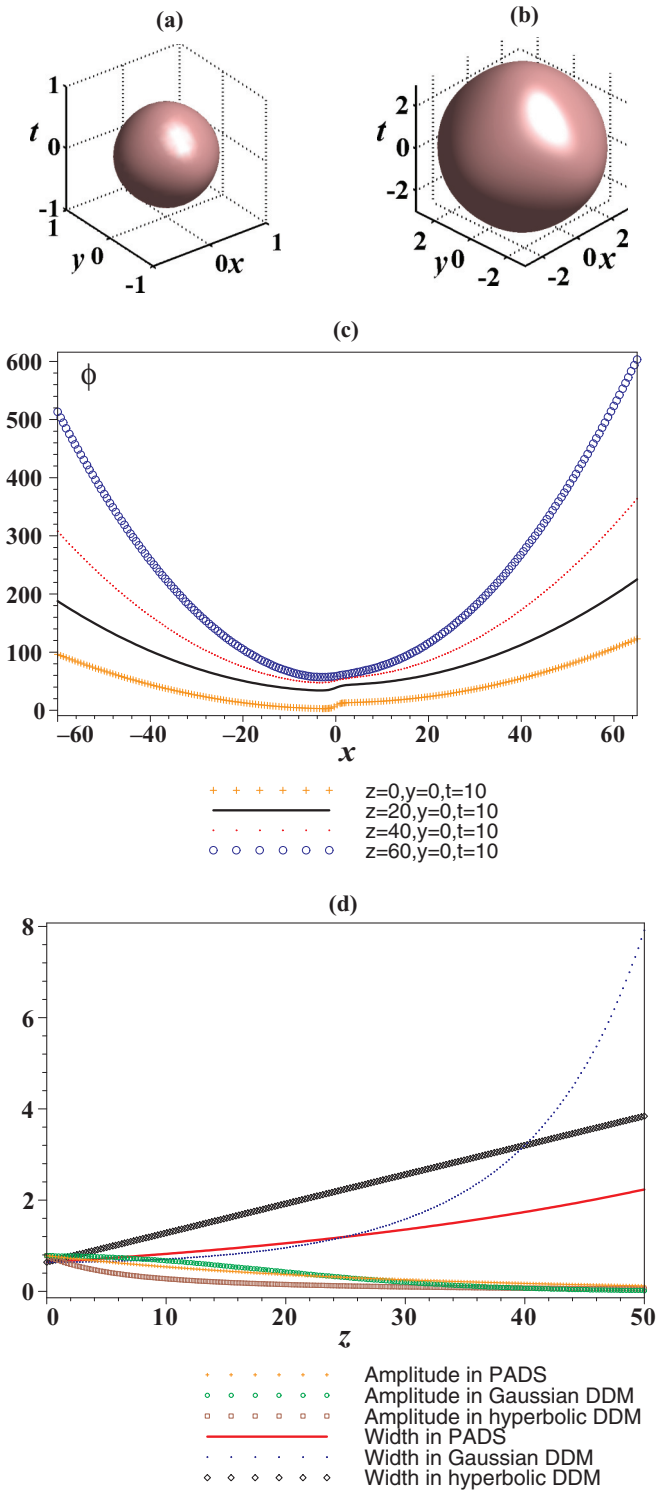

FIG. 3. (Color online) Isosurface plots of broadened LBs in PDAS at (a) $z = 0$ and (b) $z = 50$. (c) Phase change along the propagation distance z. (d) The comparison of amplitude and width of LB in different systems. The parameters are chosen as $\beta_0 = 0.5$, $\chi_0 = 0.3$, $\delta = 0.025$, $\sigma = 0.02$, $B = 2$, $G = 1$, $\rho_0 = 0.4$, $W_0 = 10$, $V_0 = 1$, $C = 5$, $L = 40$.

Figs. 2(c) and 2(d) is gradually compressed along the propagation distance z. The amplitude of LB increases little by little, while the width gradually decreases. Figure 3(e) exhibits the phase change to this case in the x-y plane. The phase of LB is expressed as $\phi = \omega_z/[2\beta(z)\omega(z)] + 3Z + W_0\{\arctan[\sinh(X)] + \arctan[\sinh(Y)] + \arctan[\sinh(T)]\}/3$, which is a result of the superposition of the chirped phase (parabolic shape) and the abrupt phase transition similarly to Fig. 1(b). Therefore, the phase shows a change at $x = 0$ or $y = 0$ on the parabolic background from small value in the negative x or y axis to big value in the positive x or y axis.

Besides the compressed LB, we can discuss the broadened LB in a periodic distributed amplification system (PDAS) with $\beta(z) = \beta_0 \exp(-\delta z)\chi(z)$, $\chi(z) = \chi_0 + \chi_1 \sin(\sigma z)$ [31], where constants β_0, δ, χ_0, χ_1, and σ have similar meanings to those in DDM. From Figs. 3(a) and 3(b), LB is gradually broadened along the propagation distance z, and the phase change will also appear. This phase change is also a result of the superposition of the chirped phase and the abrupt phase transition similar to Fig. 1(b). Along the propagation distance z, the value of the chirped phase adds little by little, and the influence of the abrupt phase transition on total phase ϕ gradually attenuates, as shown in Fig. 3(c).

Moreover, LB (2) with (15) is also broadened when it propagates in the hyperbolic DDM $\beta(z) = \beta_0\{L/[(C-1)z + L]\}\chi(z)$, $\chi(z) = \chi_0 + \chi_1 \sin(\sigma z)$ [32,33] and the Gaussian DDM $\beta(z) = \beta_0 \exp[-\ln(C)(z/L)^2]\chi(z)$, $\chi(z) = \chi_0 + \chi_1 \sin(\sigma z)$ [32,34]. Parameter C is the inverse of the compression ratio parameter, L denotes length of the medium, and other parameters are same as those in PDAS. Figure 3(d) exhibits the comparison of amplitude and width of LB in different DDMs. LB has the biggest stretch when it propagates along the hyperbolic DDM and the smallest stretch when it propagates along the PADS. However, the change of amplitude has a different case. Within the distance $z = 0$ and $z = 25$, the amplitude of LB decreases fastest in the hyperbolic DDM and slowest in the Gaussian DDM. From $z = 25$ to $z = 40$, the amplitude of LB decreases fastest in the hyperbolic DDM and slowest in the PDAS. From $z = 40$ to $z = 50$, the amplitude of LB decreases fastest in the Gaussian DDM and slowest in the PDAS.

In self-defocusing media, we can also find the compression and broadened behaviors of LB (2) with (16). The evolutional behaviors of the intensity in self-defocusing media are similar to that above discussion in self-focusing media; however, the phase change has opposite case. As shown in Figs. 2(e) and 3(c), the phase change at $x = 0$ or $y = 0$ from a small value in the negative x or y axis to a big value in the positive x or y axis. In self-defocusing media, the phase change at $x = 0$ or $y = 0$ is from big value in the negative x or y axis to small value in the positive x or y axis [see Fig. 4(a)].

Similarly to LB in Figs. 3(a) and 3(b), the broadened behavior of LB (2) with (16) in PDAS can also been found. However, the phase of LB (2) with (16) in PDAS is different from that in Fig. 3(c). The parabolic shape opens downward in this case, and the phase change at $x = 0$ or $y = 0$ is also from big value in the negative x or y axis to small value in the positive x or y axis. In this example, the complex PT-symmetric potentials in Figs. 4(c) and 4(d) have different profiles compared with those in Figs. 2(a) and 2(b). There is a symmetric relation between the profiles in Figs. 4(c) and 4(d) and Figs. 2(a) and 2(b). Obviously, here $v(x,y,t)$ and $w(x,y,t)$ still satisfy the properties of even and odd

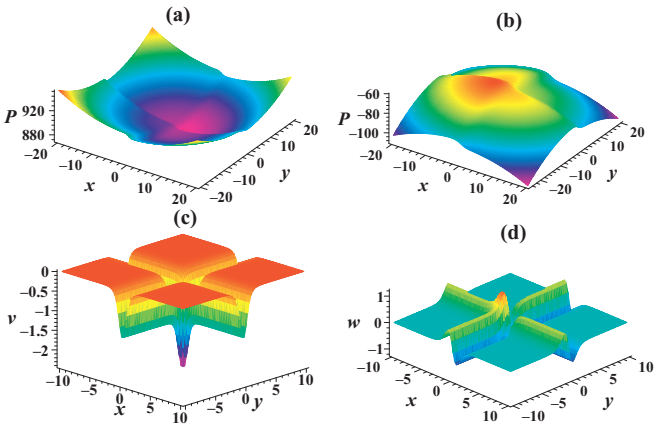

FIG. 4. (Color online) Phase changes of LB (2) with (16) in (a) the exponential DDM and (b) PDAS. The profiles of (c) even function v and (d) odd function w at $t = 10$ in PDAS. The parameters are chosen as (a) $\beta_0 = 0.5$, $\chi_0 = -0.3$, $\delta = 0.025$, $\sigma = 0.02$, $B = 2$, $G = -1$, $\rho_0 = 1$, $V_1 = 10$, $V_2 = 3$; and (b)–(d) $\beta_0 = -0.5$, $\chi_0 = 0.5$, $\chi_1 = 0.3$, $\delta = 0.025$, $\sigma = 0.02$, $B = -2$, $G = 1$, $\rho_0 = 0.4$, $V_1 = -10$, $V_2 = -1$.

functions, respectively, with regards to x, y, and t, that is, $v(x,y,t) = v(-x,-y,-t)$ and $w(x,y,t) = -w(-x,-y,-t)$.

V. STABILITY OF LB SOLUTIONS

In the following, we discuss the stability of analytical LB solutions. The stability of analytical solutions has important values in the realistic application because only stable solutions can be found in the experiment. The current situation is somewhat confusing and even controversial. Some authors reported that the spatiotemporal pulses spread out or collapse [35]. Alexandrescu *et al.* [36] also pointed out that the stabilization of solutions in both scalar and vectorial layered media is difficult to achieve due to the irreversibility of the internal energy flows between the wave substructures, e.g., rings and peaks, during propagation. Most of them consider the stability of radially symmetric structures and do not include the modulation of diffraction. However, other authors verified that it is possible to obtain stable LB solutions with modulating the diffraction or dispersion and the nonlinearity [19,37,38].

Moreover, in order to avoid the problem of three-dimensional beam collapse, some mechanisms have been presented, such as a saturable nonlinearity [39] or an optical cavity [40]. Stable 3D dissipative localized structures or LBs have also been studied in the nonlinear Kerr cavity [41], in the type II second-harmonic generation [42], and in the optical parametric oscillator [43]. However, our situation is different: The modulation of the diffraction or dispersion, the nonlinearity, and PT-symmetric potentials are altogether affected concurrently.

We start from the linear stability analysis for Eq. (5). We consider a perturbation of an exact solution [44,45] $U(Z,X,Y,T) = \{U_n(X,Y,T) + \epsilon[R(X,Y,T) + I(X,Y,T)]\exp(i\delta Z)\}\exp(i\lambda Z)$ of Eq. (5), where ϵ is an infinitesimal amplitude, $U_n(X,Y,T)$ is a respective eigenmode [a solution of Eqs. (9) and (10)], and $R(X,Y,T)$ and $I(X,Y,T)$

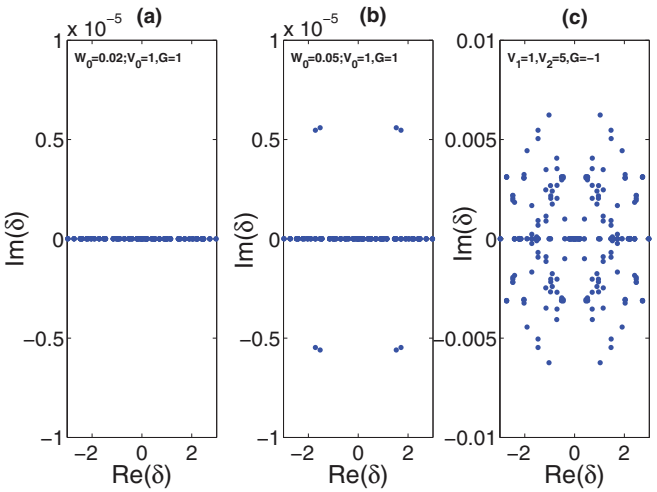

FIG. 5. (Color online) Eigenvalue for different cases: (a),(b) self-focusing nonlinearity; (c) self-defocusing nonlinearity.

are the real and imaginary parts of perturbation eigenfunctions, which may grow upon propagation with the perturbation growth rate δ. Inserting this expression into Eq. (5) and linearizing it around the unperturbed one (the first-order term of ϵ), we arrive at the eigenvalue problem

$$L_+ R = \delta I,$$
$$L_- I = \delta R, \tag{19}$$

where δ is an eigenvalue and R and I are eigenfunctions with Hermitian operators $L_+ = -\frac{B}{2}(\partial_{XX} + \partial_{YY} + \partial_{TT}) - 3GU_n(X,Y,T)^2 - (V + iW) + \lambda$ and $L_- = -\frac{B}{2}(\partial_{XX} + \partial_{YY} + \partial_{TT}) - GU_n(X,Y,T)^2 - (V + iW) + \lambda$. The linear stability of a soliton is decided by the nature of the spectrum of the above eigenvalue problem (19). If any eigenvalue δ has an imaginary part, the perturbed solution would grow exponentially with Z and thus corresponding solitons become linearly unstable. On the contrary, when all imaginary parts of δ are equal to zero, solutions can be completely stable.

Numerical calculations reveal that in the self-focusing nonlinearity for $V_0 = 1$ these localized modes are stable below the threshold $W_0 \sim 0.021$. For $W_0 > 0.021$, the corresponding localized modes become unstable. Figures 5(a) and 5(b) display the real and imaginary parts of both the stable and the unstable localized solutions below and above this threshold. Linear stability analysis of the localized modes corresponding to self-defocusing nonlinearity reveals that these modes are always unstable for all V_1 and V_2. A numerical solution of the eigenvalue problem (19) has been shown in Fig. 5(c), which also implies that the corresponding modes are linearly unstable.

In the following, we study analytical solutions evolving along distance when they are disturbed from their analytically given forms for Eq. (1). We perform a direct numerical simulation, a 3D split-step Fourier technique, adapted for z-dependent coefficients, with initial white noise for Eq. (1) with initial fields coming from the transformation (2) and solutions (15) and (16) in some cases. Four examples of such behaviors are exhibited in Fig. 6.

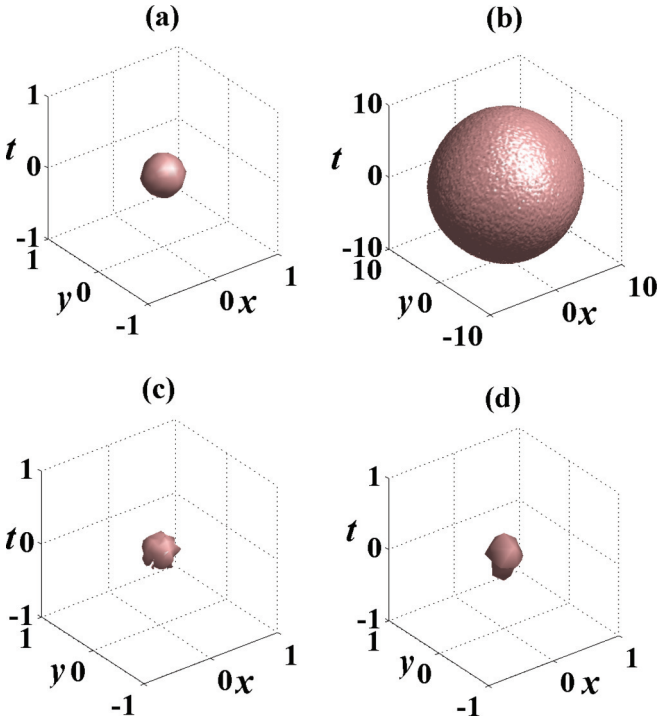

FIG. 6. (Color online) (a),(b) Stable LBs for Fig. 5(a) in the exponential DDM and PADS corresponding to Figs. 2 and 3 at $z = 100$. (c),(d) Unstable LBs for Figs. 5(b) and 5(c) in the exponential DDM corresponding to Figs. 2 and 4 at $z = 100$. An added 5% white noise is added to the initial values. The parameters are the same as those in the corresponding analytical plots except for these parameters marked in Fig. 5.

Figures 6(a) and 6(b) essentially present the numerical rerun of LBs corresponding to Fig. 2 at $z = 100$ and Fig. 3 at $z = 100$ except for these parameters marked in Fig. 5(a). The numerical solution does not give to any visible instability, and good agreement with analytical solutions is observed. Numerical calculations indicate no collapse, and stable propagations over 100 diffraction or dispersion lengths are observed except for some small oscillations. Moreover, LB is more stable in the PDAS than in the DDM because only small oscillation of surface for LB appears in Fig. 6(b), but a very small distortion exists in Fig. 6(a). As the coefficients are trigonometric functions in the PDAS, the sign-changing nonlinearity is produced, and this leads to a more stable solution shown in Fig. 6(b). Figs. 6(c) and 6(d) exhibit unstable LBs for Figs. 5(b) and 5(c) in the exponential DDM corresponding to Figs. 2 and 4 at $z = 100$. As expected, LBs which are predicted to be unstable in Figs. 5(b) and 5(c) cannot maintain their original shapes, distort and collapse, and ultimately decay into noise.

From these analysis above, we know that in the complex PT-symmetric potential of the Scarff II type expressed as (11) and (12), for a certain V_0, the value of W_0 should be much smaller than that of V_0, which influences the structure of the index guiding. More important, the value of W_0 shows that the gain (loss) should be enough small; otherwise, any small fluctuations of the field are amplified (absorbed), eventually leading to instability. Moreover, for the same parameters of the complex PT-symmetric potential (i.e., W_0 and V_0), the sign-changing nonlinearity in PADS leads to a more stable solution than that in the DDM. It is seen that after the application of diffraction or dispersion management LBs remain stable for larger propagation distances. This shows clearly the effect of the oscillating diffraction or dispersion coefficient on the wave stabilization.

VI. CONCLUSIONS

In summary, we review the main points offered in this paper.

(i) Analytical LB solutions are obtained and tested by means of direct simulations. We obtain analytical LB solutions of a 3D NLSE with inhomogeneous diffraction or dispersion and nonlinearity in the presence of the harmonic and parity-time symmetric potentials. Diffraction or dispersion and nonlinearity play important roles in the evolutional characteristics including amplitude, width, and phase. The numerical rerun to analytical solutions does not give to any visible instability, and good agreement with analytical solutions is observed.

(ii) The compression and broadening behaviors of LBs are studied. The compression and broadening behaviors of LBs are discussed and compared in the exponential, Gaussian, and hyperbolic DDM and the PDAS. Moreover, phase changes of LBs in different systems are also illustrated. These phase changes are the result of the superposition of the chirped phase and the abrupt phase transition similarly to Fig. 1.

These results are potentially useful for future experiments and applications of synthetic PT-symmetric systems.

ACKNOWLEDGMENTS

This work was supported by the National Natural Science Foundation of China (Grants No. 11375007 and No. 11375079), the Zhejiang Provincial Natural Science Foundation of China (Grant No. LY13F050006), and the Scientific Research and Developed Fund of Zhejiang A & F University (Grant No. 2013FR065). Dr. Chao-Qing Dai is also sponsored by the Foundation of New Century "151 Talent Engineering" of Zhejiang Province of China.

[1] C. M. Bender and S. Boettcher, Phys. Rev. Lett. **80**, 5243 (1998).
[2] C. M. Bender, D. C. Brody, and H. F. Jones, Phys. Rev. Lett. **89**, 270401 (2002).
[3] D. N. Christodoulides, F. Lederer, and Y. Silberberg, Nature (London) **424**, 817 (2003).
[4] E. A. Ultanir, G. I. Stegeman, D. Michaelis, C. H. Lange, and F. Lederer, Phys. Rev. Lett. **90**, 253903 (2003).
[5] Z. H. Musslimani, K. G. Makris, R. El-Ganainy, and D. N. Christodoulides, Phys. Rev. Lett. **100**, 030402 (2008).

[6] K. G. Makris, R. El-Ganainy, D. N. Christodoulides, and Z. H. Musslimani, Phys. Rev. Lett. **100**, 103904 (2008).

[7] A. Guo, G. J. Salamo, D. Duchesne, R. Morandotti, M. Volatier-Ravat, V. Aimez, G. A. Siviloglou, and D. N. Christodoulides, Phys. Rev. Lett. **103**, 093902 (2009).

[8] C. E. Ruter, K. G. Makris, R. El-Ganainy, D. N. Christodoulides, M. Segev, and D. Kip, Nat. Phys. **6**, 192 (2010).

[9] S. Klaiman, U. Günther, and N. Moiseyev, Phys. Rev. Lett. **101**, 080402 (2008).

[10] F. Lederer, G. I. Stegeman, D. N. Christodoulides, G. Assanto, M. Segev, and Y. Silberberg, Phys. Rep. **463**, 1 (2008).

[11] Z. W. Shi, X. J. Jiang, X. Zhu, and H. G. Li, Phys. Rev. A **84**, 053855 (2011).

[12] V. Achilleos, P. G. Kevrekidis, D. J. Frantzeskakis, and R. Carretero-González, Phys. Rev. A **86**, 013808 (2012).

[13] W. P. Zhong, M. R. Belić, and T. W. Huang, Nonlinear Dyn. **70**, 2027 (2012).

[14] X. Lü and M. Peng, Nonlinear Dyn. **73**, 405 (2013).

[15] W. P. Zhong, R. H. Xie, M. Belić, N. Petrović, and G. Chen, Phys. Rev. A **78**, 023821 (2008)

[16] C. Q. Dai, Y. Y. Wang, and J. F. Zhang, Opt. Lett. **35**, 1437 (2010).

[17] Y. X. Chen and X. H. Lu, Opt. Commun. **285**, 3890 (2012).

[18] Z. Y. Yan, V. V. Konotop, and N. Akhmediev, Phys. Rev. E **82**, 036610 (2010).

[19] M. Belić, N. Petrović, W. P. Zhong, R. H. Xie, and G. Chen, Phys. Rev. Lett. **101**, 123904 (2008).

[20] S. H. Chen and J. M. Dudley, Phys. Rev. Lett. **102**, 233903 (2009).

[21] B. A. Malomed, D. Mihalache, F. Wise, and L. Torner, J. Opt. B **7**, R53 (2005).

[22] V. N. Serkin, A. Hasegawa, and T. L. Belyaeva, Phys. Rev. Lett. **98**, 074102 (2007).

[23] V. N. Serkin and A. Hasegawa, Phys. Rev. Lett. **85**, 4502 (2000); JETP Lett. **72**, 89 (2000); V. N. Serkin, A. Hasegawa, and T. L. Belyaeva, Phys. Rev. A **81**, 023610 (2010); V. N. Serkin, A. Hasegawa, and T. L. Belyaeva, J. Mod. Opt. **57**, 1456 (2010).

[24] J. C. Liang, H. P. Liu, F. Liu, and L. Yi, J. Phys. A: Math. Theor. **42**, 335204 (2009).

[25] N. Z. Petrovic, M. Belic, and W. P. Zhong, Phys. Rev. E **81**, 016610 (2010).

[26] Y. Y. Wang and C. Q. Dai, Commun. Theor. Phys. **58**, 255 (2012).

[27] C. Q. Dai, R. P. Chen, and J. F. Zhang, Chaos, Solitons Fractals **44**, 862 (2011).

[28] Z. H. Musslimani, K. G. Makris, R. El-Ganainy, and D. N. Christodoulides, J. Phys. A: Math. Theor. **41**, 244019 (2008).

[29] V. I. Kruglov, A. C. Peacock, and J. D. Harvey, Phys. Rev. Lett. **90**, 113902 (2003).

[30] R. Yang, R. Hao, L. Li, X. Shi, Z. Li, and G. Zhou, Opt. Commun. **253**, 177 (2005).

[31] R. Hao, L. Li, Z. Li, W. Xue, and G. Zhou, Opt. Commun. **236**, 79 (2004).

[32] M. G. Da Silva, K. Z. Nobrega, and A. S. B. Sombra, Opt. Commun. **171**, 351 (1999).

[33] M. Zitelli, B. Malomed, F. Matera, and M. Settembre, Opt. Commun. **154**, 273 (1998).

[34] M. N. Vinoj and V. C. Kuriakose, J. Opt. A **6**, 63 (2004).

[35] M. Matuszewski, M. Trippenbach, B. A. Malomed, E. Infeld, and A. A. Skorupski, Phys. Rev. E **70**, 016603 (2004).

[36] A. Alexandrescu, G. D. Montesinos, and V. M. Perez-Garcia, Phys. Rev. E **75**, 046609 (2007).

[37] W. P. Zhong, M. Belić, G. Assanto, and T. Huang, J. Phys. B: At. Mol. Opt. Phys. **44**, 095403 (2011).

[38] W. P. Zhong, M. Belić, G. Assanto, B. A. Malomed, and T. Huang, Phys. Rev. A **84**, 043801 (2011).

[39] N. Akhmediev and J. M. Soto-Crespo, Phys. Rev. A **47**, 1358 (1993).

[40] P. M. Lushnikov and M. Saffman, Phys. Rev. E **62**, 5793 (2000); M. Tlidi, M. Haelterman, and P. Mandel, Eur. Phys. Lett. **42**, 505 (1998).

[41] P. Tassin, G. Van der Sande, N. Veretenov, P. Kockaert, I. Veretennicoff, and M. Tlidi, Opt. Express **14**, 9338 (2006).

[42] M. Tlidi and P. Mandel, Phys. Rev. Lett. **83**, 4995 (1999); M. Tlidi, J. Opt. B: Quantum Semiclassical Opt. **2**, 438 (2000).

[43] N. Veretenov and M. Tlidi, Phys. Rev. A **80**, 023822 (2009).

[44] J. C. Bronski, L. D. Carr, B. Deconinck, and J. N. Kutz, Phys. Rev. Lett. **86**, 1402 (2001).

[45] B. Midya and R. Roychoudhury, Phys. Rev. A **87**, 045803 (2013).